ROYAL SOCIETY OF CHEMISTRY

## PAPER

Check for updates

# Solvent-free mechanochemical conversion of $CO_2$ into mesoporous SiC: a green route to high-performance catalysts

Hae In Lee,[†a] Myung Won Seo,[†b] Dong Hyun Kim,[c] Hyuk Choi, [iD][d] Ju Hyeok Lee,[d] Mi Yoo, [iD][d] Min-Jae Kim,[c] Yong-Sik Ok, [iD][e] Siddheshwar Dadarao Raut,[f] Dong Hyun Lee, [iD][f] Hyun You Kim, [iD][*d] Kyubock Lee [iD][*c] and Won-Chul Cho [iD][*f]

Silicon carbide (SiC) is a critical material across structural, electronic, and catalytic applications; however, its conventional synthesis via the Acheson process is highly energy-intensive, operating at 2200–2400 °C with low carbon efficiency. Herein, we report a novel, solvent-free mechanochemical synthesis of mesoporous SiC using $CO_2$ as a sustainable carbon feedstock and $SiO_2$/Mg as earth-abundant precursors. Through a two-step ball-milling process, $SiO_2$ is first reduced by Mg to form $Mg_2Si$, which then spontaneously reacts with $CO_2$ to form SiC and MgO, achieving a high $CO_2$ conversion efficiency of 84% at only 10% of the energy cost of conventional methods. Density functional theory (DFT) calculations confirm the thermodynamic feasibility of $CO_2$ activation on $Mg_2Si$. The produced mesoporous SiC exhibited excellent durability and served as a highly stable support for Ni catalysts in dry reforming of methane ($CH_4$ + $CO_2$ → $H_2$ + CO), maintaining performance over 100 hours with minimal coke formation. This work introduces a green, scalable route for synthesizing high-value SiC, integrating $CO_2$ utilization and catalyst development under the principles of green chemistry.

[a]School of Energy and Chemical Engineering, Ulsan National Institute of Science and Technology, Ulsan 44919, Republic of Korea

[b]School of Environmental Engineering, University of Seoul, Seoul 02504, Republic of Korea

[c]Graduate School of Energy Science & Technology, Chungnam National University, Daejeon 34134, Republic of Korea. E-mail: kyubock.lee@cnu.ac.kr

[d]Department of Materials Science and Engineering, Chungnam National University, Daejeon 34134, Republic of Korea. E-mail: kimhy@cnu.ac.kr

[e]Korea Biochar Research Center & Division of Environmental Science and Ecological Engineering, Korea University, Seoul 02841, Republic of Korea

[f]Department of Future Energy Convergence, Seoul National University of Science & Technology, Seoul 01811, Republic of Korea. E-mail: wonchul.cho@seoultech.ac.kr

† These authors contributed equally to this study.

## Introduction

Nature supports the ecosystem by utilizing $CO_2$ as a carbon feedstock to synthesize carbohydrates. However, because our current civilization cannot efficiently upgrade $CO_2$ to valuable chemicals, we face a gradual but inevitable accumulation of $CO_2$ in the atmosphere. Consequently, the amount of $CO_2$ accumulated in the atmosphere has reached approximately 20 Gt $CO_2$ per year,[1] motivating the immediate application of $CO_2$ capture and storage technologies. The current strategies for mitigating climate change driven by anthropogenic $CO_2$ emissions involve direct $CO_2$ sequestration in sedimentary rocks or saline aquifers and $CO_2$ mineralization.[2–6] However, despite the leakage-free compact $CO_2$-sequestration route provided by $CO_2$ mineralization to alkaline earth metal carbonates, the process sites are spatially limited to locations at which sufficient geological storage capacity of carbonates is ensured for underground sequestration. Unfortunately, this spatial limitation concurrently applies to direct $CO_2$ injection technologies.[7,8]

Here, we instead formulate a concrete economic value chain covering efficient $CO_2$ conversion to value-added products. We focus on silicon carbide, SiC, a vital material in structural, electronic, and energy applications, to maximize the economic impact.[9] Commercial SiC powders are typically produced by the energy-consuming Acheson process ($SiO_{2(s)}$ + $3C_{(s)}$ → $SiC_{(s)}$ + $2CO_{(g)}$).[10] The Acheson process lasts for several hours (up to 30 h) and involves a long, direct carbothermic reaction of quartz sand and petroleum with low commercial yields of ~19% at extremely high temperatures (~2200–2400 °C).[11] A general Acheson process consumes 7300–7600 kW h of energy to produce a metric ton of SiC, equivalent to the total energy stored in approximately 100 fully charged electric vehicles.[12] Moreover, because the produced α-SiC particles are large and highly crystalline, mechanical milling and subsequent conversion into relatively novel β-SiC powders through carbothermic reduction should be performed.[13] The quality of the produced SiC can be improved using higher-grade resources such as a stoichiometric mixture of metallic Si particles of $d$ < 20 μm and C powders for carbothermic reduction[14] or a mixture of activated C and Si (or silica) for microwave processing.[15] However, these approaches are also time-consuming and cost-ineffective.

Inspired by the mechanochemical conversion method,[16–19] we designed a straightforward and cost-effective method of synthesizing high-quality SiC using $CO_2$ as a carbon resource. In this approach, a mixture of nano-$SiO_2$ particles (nsp) and Mg is initially converted into $Mg_2Si$, a key intermediate, *via* ball-milling. The strong interaction between $Mg_2Si$ and $CO_2$ activates the subsequent transformation of $Mg_2Si$ into mesoporous SiC. The advanced multifunctional SiC synthesis reported herein provides an intelligent route for producing high-quality SiC with a high carbon conversion efficiency of 84%. Our mechanochemical synthesis method provides a means of directly utilizing $CO_2$ in value-added metal carbides. In addition, the applicability and quality of our mechanochemically produced mesoporous SiC were confirmed by the excellent efficiency and consistency of the Ni/SiC catalysts toward dry reforming of methane (DRM).

## Results and discussion

Mechanochemical conversion is based on ball-milling, which initiates the reaction without significant energy consumption. If the overall process is well-designed, then the ball-milling-based conversion process is energetically efficient as the reaction proceeds inside the mechanically robust chamber in an adiabatic manner. We emphasize that our multi-step mechanochemical SiC synthesis method uses Mg and $Mg_2Si$ as reaction initiators for the first and second milling processes. Based on the inherent high reactivity of Mg and $Mg_2Si$, we designed the two-step mechanochemical synthesis of SiC from $SiO_2$, regarding Mg and $Mg_2Si$ as a reaction activator and an energy source.

Fig. 1a provides a schematic of a two-step, ball-milling-based sequential mechanochemical SiC synthesis process. During the reaction, Mg reduces $SiO_2$-nsp and produces $Mg_2Si$, a crucial substance in the overall process. The second subsequent mechanochemical reaction converts a mixture of $Mg_2Si$ and $CO_2$ into SiC and MgO. The high-resolution transmission electron microscopy (HR-TEM) images reveal the morphology of the produced SiC-nsp particles (Fig. 1b–d). The synthesized SiC-nsp particles exhibit mesoporous textures composed of single-crystalline primary SiC nanoparticles with a typical [111] interlayer spacing of β-SiC (0.252 nm) (Fig. 1b–d and SI Fig. 1 and 2).

The density functional theory (DFT)-calculated energetics of $CO_2$ binding and dissociation on the surface of $Mg_2Si$ nanoparticles confirm that $Mg_2Si$ binds and activates $CO_2$ (Fig. 1e). Up to 10 $CO_2$ molecules are exothermically bound to a single $Mg_2Si$ nanoparticle ($E_{bind}$ = −1.69 eV per $CO_2$), and the subsequent dissociation steps are thermodynamically driven with $\Delta E$ = −1.18 eV per $CO_2$, which originates from the atomic-scale formation of SiC and MgO units within the matrix of a $Mg_2Si$ nanoparticle (Fig. 1e). Additional calculations performed with three representative $Mg_2Si$ surfaces reveal that the binding and dissociation of $CO_2$ on $Mg_2Si$ is energetically feasible (SI Fig. 3).

The reaction pressure profile presented as a function of the reaction time shows that the conversion occurs fairly rapidly after 150 s of incubation time (Fig. 2a). The X-ray diffraction (XRD) spectra show that $Mg_2Si$ and MgO are the primary products of the first ball-milling step (Fig. 2b). The pressure–reaction time profile presented in Fig. 2c demonstrates that the second conversion is completed within 40 s, generating a mixture of SiC and MgO from $Mg_2Si$ and $CO_2$. Note that $CO_2$ is the sole carbon resource for the carbonization of $Mg_2Si$ to SiC.
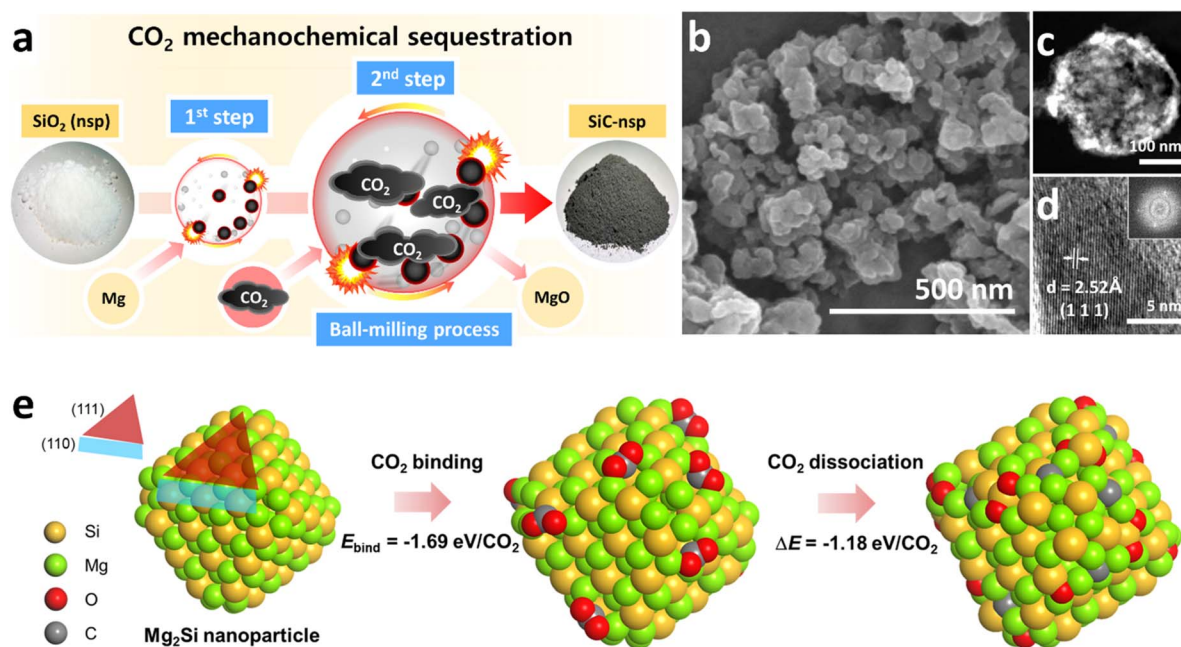


Fig. 1 Ball-milling-based mechanochemical SiC synthesis. (a) Illustration of the ball-milling process and images of the nsp and SiC-nsp powders, (b) SEM, (c) STEM, and (d) HR-TEM images of SiC-nsp, (e) DFT-calculated energetics of $CO_2$ activation and dissociation on an $Mg_2Si$ nanoparticle. $E_{bind}$ denotes the average binding energy of $CO_2$ on the $Mg_2Si$ nanoparticle.
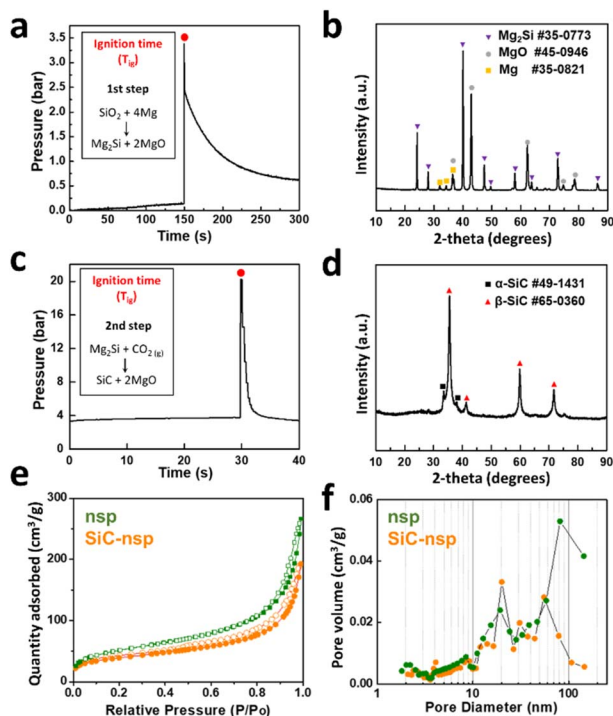
**Fig. 2** Reaction profile and structural analysis of the intermediates and final products. (a) Ignition time and pressure changes in the milling vial during the first step, (b) XRD pattern of the prepared powder after the first step, (c) ignition time and pressure changes during the second step of milling, (d) XRD pattern of the finally produced SiC-nsp, (e) $N_2$-adsorption–desorption isotherms of nsp and SiC-nsp, and (f) BJH pore diameter distributions of nsp and SiC-nsp.

Remarkably, the reaction proceeds adiabatically without any energy supply from the outside. The final product, SiC-nsp, was obtained after sequential acid-base leaching. The XRD pattern of the finally produced SiC powder confirms the primary peaks of β-SiC. No amorphous carbon layer (ACL) was found on the surface of SiC-nsp (SI Fig. 2).

The $N_2$ adsorption–desorption isotherms of nsp and SiC-nsp are shown as type-II profiles (Fig. 2e). The overall trend of the hysteresis loops of nsp and SiC-nsp displays a typical type-H3 profile, which represents non-rigid aggregates of particles, consistent with the electron microscope observations (SI Fig. 1), while the H3 hysteresis also suggests additional interparticle voids that can extend toward the macropore regime. The Barrett–Joyner–Halenda (BJH) pore-size distributions reveal that the mesopore structures of nsp and SiC-nsp are similar to each other (Fig. 2f). The decreased surface area and pore volume of SiC-nsp (140 $m^2 g^{-1}$ and 0.30 $cm^3 g^{-1}$, respectively) compared to those of nsp (195 $m^2 g^{-1}$ and 0.41 $cm^3 g^{-1}$, respectively) are presumably due to the slight particle aggregation that occurred during ball milling (SI Tables 1 and 2). The similar morphological features in the $N_2$ adsorption–desorption isotherms and the BJH pore diameter distribution profiles of nsp and SiC-nsp show that the initial microstructure of the $SiO_2$ resource (nsp) is conserved in the final mechanochemically produced SiC (SiC-nsp). Our mechanochemical conversion method provides

a novel route toward intentional control of the morphology of SiC, based on efficient conversion of $SiO_2$ through the solid–gas reaction, which is not available in the commercial Acheson process by the solid–solid reaction.

Value-added porous sub-micron SiC powders (approximately USD 300 per kg) could be produced by our mechanochemical synthesis using low-cost and readily available commercial materials such as nano-$SiO_2$ (USD 2 per kg), Mg (USD 10 per kg), and $CO_2$ (USD 0.06 per kg) via simple milling processes. An almost stoichiometric amount of $CO_2$ was utilized to produce SiC; 3.4 g of SiC was obtained from 4.4 g of $CO_2$, corresponding to a yield of 84% for $CO_2$–SiC conversion.

To explore the versatility of our mechanochemical SiC synthesis method, we repeated the two-step ball-milling process using a naturally porous rice husk silica (rha) as a biomass-based alternative owing to its large-scale global availability (~70 million tons were produced in 2012). The XRD patterns, scanning electron microscopy (SEM) images, and TEM images concurrently confirm that porous SiC (SiC-rha) is produced using rha as the $SiO_2$ source (Fig. 3a and SI Fig. 4). These findings suggest that our mechanochemical SiC synthesis method is highly versatile and adaptable to various situations, regardless of the quality and type of the $SiO_2$ source. We further applied the conventionally used powder-activated carbon (AC) instead of $CO_2$ as a carbon source in the ball-milling cycle with the nsp. The SiC synthesized with AC (SiC-nsp-ac) exhibits a higher Si peak intensity in the XRD spectra (SI Fig. 5), suggesting a lower conversion efficiency of solid-phase AC compared to gaseous $CO_2$. In addition, the unreacted AC during the milling process generates an ACL on the surface of SiC-nsp-ac (Fig. 3c). The thermogravimetric analysis (TGA) curve shows that the SiC-nsp-ac undergoes noticeable weight loss between 460 °C and 550 °C, which can be attributed to the oxidation of the residual carbon (Fig. 3d). Our
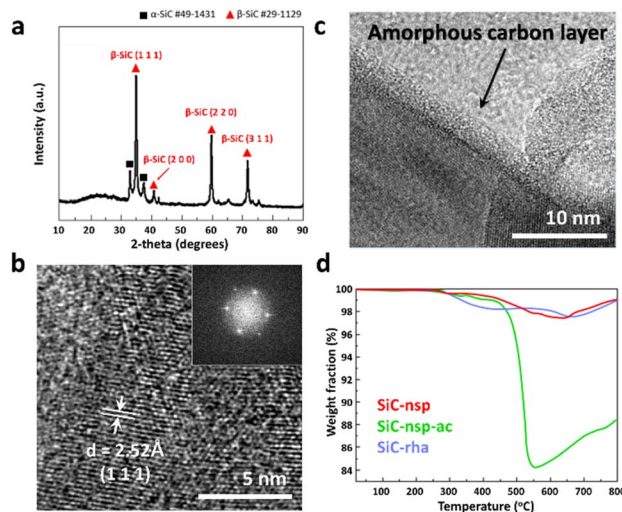


**Fig. 3** Morphology of SiC powders produced from different starting materials. (a) XRD pattern of SiC-rha, (b) corresponding TEM image, (c) TEM image showing the ACL of the SiC-nsp-ac sample, and (d) TGA curves of the synthesized SiC with different starting materials.

results show that reactive $Mg_2Si$ intermediate enables gaseous $CO_2$ to interact vigorously with solid substances despite its general chemical inertness.

Chemical durability is among the key strengths of SiC in industrial applications.[20] The surface area and elemental composition of the mechanochemically produced SiC presented herein do not show any considerable changes after exposure to harsh acidic and basic conditions for three weeks (SI Table 3). Based on the inherent physicochemical robustness of SiC, various promising catalytic reactions have been performed using $\beta$-SiC as a catalyst or catalyst support.[21–25] One of the key characteristics of a catalyst or catalyst support is a high surface area that has hardly been achieved for $\beta$-SiC produced through the high-temperature Acheson process.[11] We applied the mechanochemically produced mesoporous SiC-nsp as a support for Ni-based DRM catalysts (Ni/SiC-nsp, specific surface area = 79 $m^2$ g; SI Table 4) that convert the two most significant greenhouse gases ($CH_4$ and $CO_2$) into industrially valuable syngas ($H_2$ and CO).[26–28]

Therefore, we suggest a two-step sequential $CO_2$ utilization process via mechanochemical SiC synthesis followed by DRM catalysis by Ni/SiC-nsp, as shown in Fig. 4a. The TEM and energy-dispersive X-ray spectroscopy mapping images of the catalysts after Ni and Mg impregnation as the active sites and promotors reveal homogeneously dispersed Ni nanoparticles with an average size of 19.7 nm on the SiC support (Fig. 4b). The homogeneous dispersion and fine particle size of the active sites originate from the mesoporosity of SiC. The DRM reaction test results in Fig. 4c show that the Ni/SiC-nsp catalyst consistently catalyzes the DRM reaction with the $CH_4$ and $CO_2$ conversions close to thermodynamic equilibrium for 100 h without significant reduction.

Remarkably, the resistance against coke deposition of the catalyst, the most significant challenge hindering the commercialization of DRM catalysts, evaluated by TGA after 100 h of reaction revealed only 1.71 wt% coke deposition on the Ni/SiC-nsp, which corresponds to 0.174 $mg_{coke}$ $g_{cat}^{-1}$ $h^{-1}$ (Fig. 4d). These results demonstrate the superior performance of SiC-nsp as a catalyst support for high-temperature reactions. The stability and coke resistance of Ni/SiC-nsp (as indicated by the red star symbol) is compatible with the recently reported high-performance DRM catalysts (as denoted by the black rectangular symbols), prevailing those of the previously reported SiC-based Ni catalyst (red rectangular symbol).[29–40] For large-scale and high-temperature catalysis, overcoming cold or hot spots on the catalyst bed and enduring thermal shocks during operation are of great importance for the performance and stability of the catalytic reaction. Considering that the most fascinating characteristics of SiC as the catalyst or catalyst support are its high thermal conductivity and stability,[41,42] our mesoporous SiC is highly applicable in various catalytic systems.
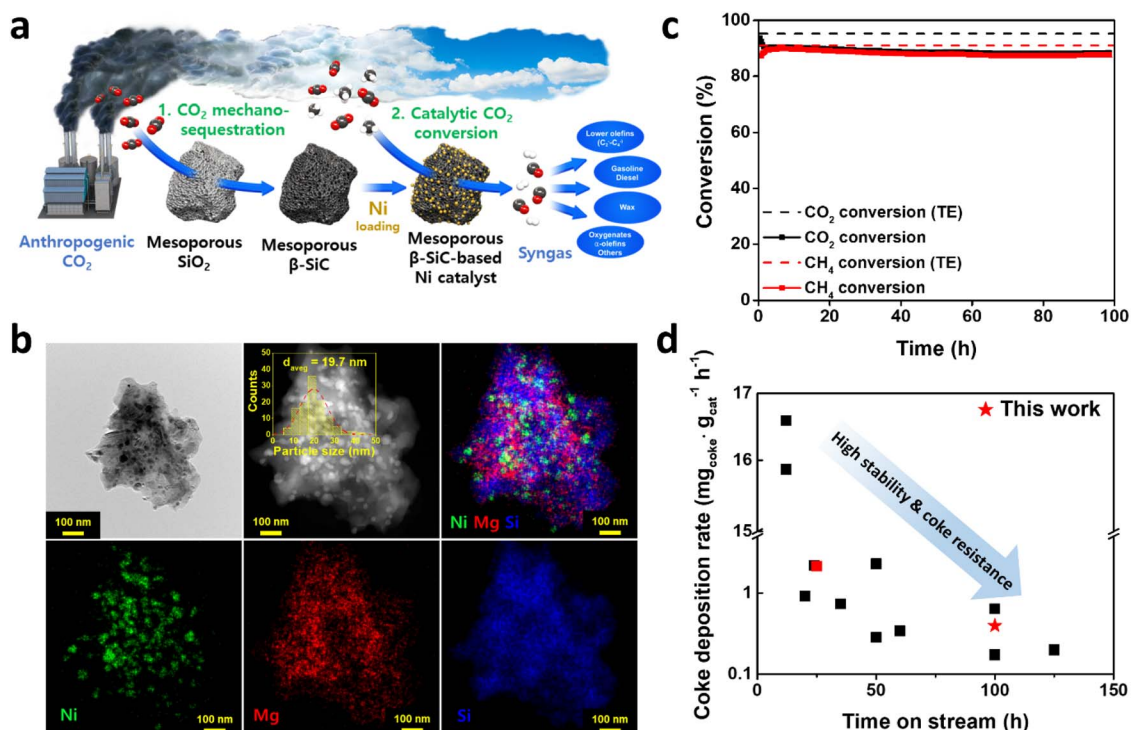


Fig. 4 Mesoporous Ni/SiC catalysts in the DRM reaction. (a) Schematic diagram of a two-step sequential $CO_2$ utilization process via mechanochemical SiC synthesis followed by DRM catalyzed by Ni/SiC-nsp, (b) TEM images with HAADF and EDS mapping of Ni/SiC-nsp catalyst, (c) $CO_2$ and $CH_4$ conversion during a 100 h DRM reaction at 800 °C and a 10 000 mL $g^{-1}$ $h^{-1}$, of WHSV where the dashed lines indicate each conversion at thermodynamic equilibrium, (d) comparison of the stability and coke resistance of Ni/SiC-nsp with those of previously reported DRM catalysts.[25–36]
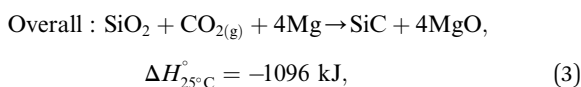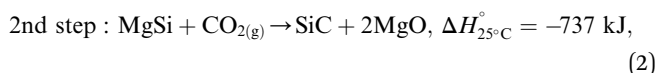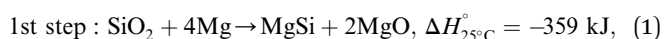
## Conclusions and outlook

In conclusion, we present a sustainable and energy-efficient route for synthesizing silicon carbide (SiC) *via* a two-step mechanochemical conversion of $SiO_2$ and $CO_2$ using Mg as a reductant. This self-activated solid–gas reaction proceeds under solvent-free conditions with minimal energy input, achieving 84% $CO_2$ conversion efficiency and producing mesoporous SiC with excellent catalytic properties. The SiC-supported Ni catalyst demonstrated high stability and coke resistance during dry reforming of methane, validating the functional applicability of the synthesized material. By utilizing earth-abundant precursors and converting $CO_2$ into a value-added product under mild conditions, our strategy aligns with the core principles of green chemistry, offering a viable path toward climate-resilient materials synthesis.

## Methods

### Preparation of silicon carbide

Our synthesis route involves the milling process, wherein both $SiO_2$ (Sigma-Aldrich 99.8%) and $CO_2$ (dry ice) are reduced using Mg powder (Sigma-Aldrich 99%) as the reducing agent. A schematic illustration of the proposed reaction pathway is provided in Fig. 1a. The synthesis of SiC material is a two-step process, based on the following reactions:

$$\text{1st step}: SiO_2 + 4Mg \rightarrow MgSi + 2MgO, \Delta H^{\circ}_{25^{\circ}C} = -359 \text{ kJ}, \quad (1)$$

$$\text{2nd step}: MgSi + CO_{2(g)} \rightarrow SiC + 2MgO, \Delta H^{\circ}_{25^{\circ}C} = -737 \text{ kJ}, \quad (2)$$

$$\text{Overall}: SiO_2 + CO_{2(g)} + 4Mg \rightarrow SiC + 4MgO,$$
$$\Delta H^{\circ}_{25^{\circ}C} = -1096 \text{ kJ}, \quad (3)$$

In our experiments, 10 mm WC balls were used with a ball-to-powder ratio (BPR) of 30. Milling was performed at 350 rpm in a 500 cc milling jar during which the reaction proceeded in two main steps for 300 s and 40 s, respectively. Firstly, stoichiometric amounts of $SiO_2$ (6 g) and Mg (9.71 g) were added in a vial in a glove box system maintained under an Ar atmosphere. The vial was subjected to milling (PULVERISETTE 5, Fritsch), and the increase in the gas pressure inside the vial was monitored as a function of the milling time (Fig. 2a). After milling for 150 s, a significant increase in the pressure was observed, indicating the progress of the reaction (1) mentioned above. The XRD analysis confirmed the formation of $Mg_2Si$ (Fig. 2b). In the second step, the milling of reaction (2) proceeded after introducing dry ice (solid $CO_2$ 4.40 g) inside the vial to produce the SiC and MgO composites (Fig. 2d). Instead of introducing $CO_2$ gas, dry ice was used as the $CO_2$ source in the Ar atmosphere to supply stoichiometric amounts of $CO_2$. The second milling step was performed after monitoring the pressure inside the vial to confirm that the dry ice had sublimated into $CO_2$ gas (Fig. 2c).

The reaction between the gas ($CO_2$) and solid particles occurs when the energy reaches a certain level inside the vial. The reaction was mainly induced by the collision energy rather than the thermal energy at high temperatures to overcome the activation barrier, a process referred to as mechanochemistry.[1] Acid and base leaching was respectively performed using 10 wt% HCl and 1 M NaOH solution for the resulting SiC–MgO composite to remove MgO and other impurities from the balls and vials, yielding the final porous SiC. Nanosilica particles ($\sim$20 nm) and rice-husk-derived $SiO_2$ were used as the Si sources, and AC (SHIRASAGI) was employed as a C source and control. AC was placed in a vial in a glove box system maintained under an Ar atmosphere.

The $CO_2$ to SiC yield is defined and calculated as follows:

$$CO_2 \text{ to SiC yield}(\%) = \frac{\left(SiC_{(gram)}/CO_{2(gram)}\right)_{\text{exp.}}}{\left(SiC_{(gram)}/CO_{2(gram)}\right)_{\text{stoich.}}} \times 100(\%), \quad (4)$$

where $(SiC_{(gram)}/CO_{2(gram)})_{\text{stoich.}}$ is the stoichiometric weight ratio of the starting elements SiC and $CO_2$ and $(SiC_{(gram)}/CO_{2(gram)})_{\text{exp.}}$ is the ratio between the weights of the SiC produced and feedstock $CO_2$.

### Catalyst synthesis and catalytic reaction

Ni/SiC-nsp was synthesized by loading 5 wt% of Ni ($Ni(NO_3)_2\cdot 6H_2O$, $\geq$98%, Sigma-Aldrich, USA) and 5 wt% of Mg ($Mg(NO_3)_2\cdot 6H_2O$, $\geq$98%, Sigma-Aldrich, USA) simultaneously on SiC-nsp using the incipient wetness impregnation method. The impregnated samples were dried at 60 °C for 2 h in air and then calcined at 550 °C for 2 h (in air). After pelletizing, crushing, and sieving, the catalysts were loaded into a 1/4-inch fixed-bed quartz reactor on 3 mm of quartz wool for DRM. Pre-reduction of the catalysts was performed at 800 °C for 2 h under a gas mixture of $H_2$ (flow rate = 10 mL min$^{-1}$) and $N_2$ (flow rate = 10 mL min$^{-1}$). The feed was composed of $CH_4$, $CO_2$, and $N_2$ in a 1 : 1 : 1 ratio flowing at a weight hourly space velocity (WHSV) of 10 000 mL g$^{-1}$ h$^{-1}$. The reactions were conducted at 800 °C for 100 h. The outlet gas was analyzed every 22 min by an online gas chromatography system equipped with a thermal conductivity detector. The conversions are as follows:

$$CH_4 \text{ conversion}(\%) = \frac{[CH_4]_{\text{in}} - [CH_4]_{\text{out}}}{[CH_4]_{\text{in}}} \times 100(\%), \quad (5)$$

$$CO_2 \text{ conversion}(\%) = \frac{[CO_2]_{\text{in}} - [CO_2]_{\text{out}}}{[CO_2]_{\text{in}}} \times 100(\%) \quad (6)$$

### DFT calculations

We performed spin-polarized DFT calculations using the Vienna *Ab initio* Simulation Package code[43] with a plane-wave basis. We employed the Perdew–Burke–Ernzerhof[44] exchange-correlation functional and the DFT-D3 van der Waals correction method[2] with the Becke–Johnson damping model to improve the reliability of the results. The interaction between the ionic core and the valence electrons was described by the projector augmented wave method.[45] The valence electron wave functions were expanded in a plane-wave basis up to an energy cut-off of 400 eV. The Brillouin zone was sampled at the $\Gamma$-point

for all the calculations. The convergence criteria for the electronic structure and atomic geometry were $10^{-4}$ eV and 0.03 eV Å$^{-1}$, respectively. We used a Gaussian smearing function with a finite temperature width of 0.2 eV to improve the convergence of states near the Fermi level.

An octahedral $Mg_{158}Si_{79}$ particle located inside a $40 \times 40 \times 40$ cell was used to study the energetics of $CO_2$ binding and the formation of $SiO_2$ and SiC. The average binding energy ($E_{bind}$) of $CO_2$ on $Mg_2Si$ and the subsequent dissociation energy ($\Delta E$) were estimated by averaging $E_{bind}$ and $\Delta E$ of a total of 10 $CO_2$ molecules. To explore the inherent $CO_2$ binding and dissociation capacity of $Mg_2Si$ further, $E_{bind}$ and $\Delta E$ were calculated on pristine $Mg_2Si$ surfaces, i.e., $Mg_2Si$ (100), $Mg_2Si$ (110), and $Mg_2Si$ (111). Next, $(3 \times 3 \times 2)$, $(3 \times 4 \times 3)$, and $(4 \times 4 \times 2)$ supercells were used to model the $Mg_2Si$ (100), $Mg_2Si$ (110), and $Mg_2Si$ (111) surfaces, respectively. The bottom-most layer of the slab model was fixed during the geometry optimization. A 15 Å thick vacuum layer was introduced to prevent interactions between the periodic slabs.

### Characterization

The microstructures of the starting materials and synthesized SiC were determined by SEM (S-4800, Hitachi). TEM images and nanoscale elemental mappings were recorded using a Tecnai F30 electron microscope, operated at an accelerating voltage of 300 kV, and a Titan Double Cs corrected TEM (Titan cubed G2 60-300, FEI) operated at 300 kV. The samples for the TEM measurements were ultrasonically dispersed in ethanol. Drops of the suspension were deposited onto a C-coated Cu grid. Before the measurements, the samples were degassed at 300 °C for 2 h. The identification of the crystalline chemical species was performed by XRD using a Rigaku D/max 2500 with Cu-Kα characteristic radiation in the 2θ range of 10–90° at a scan speed of 0.2° min$^{-1}$. The crystallite size of the Ni NPs was calculated using the Scherrer equation. TGA was conducted to estimate the thermal stability using a SETSYS 1750ev (SETARAM), with 20 mg SiC samples prepared from different starting materials. For the analysis, dry air was sent at a flow rate of 300 cm$^3$ min$^{-1}$, and the heating rate was 10 °C min$^{-1}$. In addition, the amount of coke deposited on the catalysts after the reaction was determined from the TGA curves. BET analysis was performed using a BELSORP-mini (MicrotracBEL) adsorption setup after pretreatment in a vacuum at 300 °C for 3 h. The adsorption–desorption isotherm was obtained at −196 °C. The pore-size distribution was analyzed according to BJH theory. The residual composition after the chemical durability stability test of SiC was analyzed using inductively coupled plasma–optical emission spectrometry (iCAP 6000, Thermo Scientific) to detect concentrations on the order of parts per million (mg L$^{-1}$).

## Author contributions

Hae In Lee: conceptualization, methodology, investigation, writing – original draft, visualization; Myung Won Seo: conceptualization, methodology, data curation, writing – original draft; Dong Hyun Kim: investigation, methodology, visualization; Hyuk Choi: software, formal analysis, investigation; Ju Hyeok Lee: software, formal analysis, investigation; Mi Yoo: investigation; Min-Jae Kim: investigation, methodology; Yong Sik Ok: writing – review & editing; Siddheshwar Dadarao Raut: investigation, methodology; Dong Hyun Lee: software; Hyun You Kim: methodology, software, formal analysis, data curation, writing – original draft, writing – review & editing; Kyubock Lee: methodology, data curation, writing – original draft, writing – review & editing; Won Chul Cho: conceptualization, methodology, data curation, writing – original draft, writing – review & editing, supervision.

## Conflicts of interest

The authors declare no competing interests.

## Data availability

The authors declare that the data supporting the findings of this study are available within the paper and the supplementary information (SI) file. Supplementary information is available. See DOI: https://doi.org/10.1039/d5mr00091b.

## Acknowledgements

## References

1 P. Kelemen, S. M. Benson, H. Pilorgé, P. Psarras and J. Wilcox, Front. Clim., 2019, 1, 9.

2 R. Zevenhoven and J. Fagerlund, Developments and Innovation in Carbon Dioxide (CO₂) Capture and Storage Technology: Carbon Dioxide (CO₂) Storage and Utilisation, Woodhead Publishing: Sawston, ed. M. M. Maroto-Valer, vol. 2, 2010, pp. 433–462.

3 R. Costanza, R. d'Arge, R. de Groot, S. Farber, M. Grasso, B. Hannon, K. Limburg, S. Naeem, R. V. O'Neill, J. Paruelo, R. G. Raskin, P. Sutton and M. van den Belt, Nature, 1997, 387, 253–260.

4 J. M. Matter, M. Stute, S. Ó. Snæbjörnsdottir, E. H. Oelkers, S. R. Gislason, E. S. Aradottir, B. Sigfusson, I. Gunnarsson, H. Sigurdardottir, E. Gunnlaugsson, G. Axelsson,

H. A. Alfredsson, D. Wolff-Boenisch, K. Mesfin, D. F. R. Fernandez de la Reguera Taya, J. Hall, K. Dideriksen and W. S. Broecker, *Science*, 2016, **352**, 1312–1314.

5  V. Scott, S. Gilfillan, N. Markusson, H. Chalmers and R. S. Haszeldine, *Nat. Clim. Change*, 2013, **3**, 105–111.

6  E. J. Kim, R. L. Siegelman, H. Z. H. Jiang, A. C. Forse, J. H. Lee, J. D. Martell, P. J. Milner, J. M. Falkowski, J. B. Neaton, J. A. Reimer, S. C. Weston and J. R. Long, *Science*, 2020, **369**, 392–396.

7  L. Rosa, J. A. Reimer, M. S. Went and P. D'Odorico, *Nat. Sustain.*, 2020, **3**, 658–666.

8  Y.-M. Wei, J.-N. Kang, L.-C. Liu, Q. Li, P.-T. Wang, J.-J. Hou, Q.-M. Liang, H. Liao, S.-F. Huang and B. Yu, *Nat. Clim. Chang.*, 2021, **11**, 112–118.

9  K. Powell, L. Li, A. Shams-Ansart, J. Wang, D. Meng, N. Sinclair and J. Deng, *Nat. Commun.*, 2022, **13**, 1851.

10  P. Raj, G. S. Gupta and V. Rudolph, *Thermochim. Acta*, 2020, **687**, 178577.

11  P. Kennedy and B. North, *Proc. Br. Ceram. Soc.*, 1983, **33**, 1–15.

12  W. R. Natuzanhuka, *Heliyon*, 2019, **5**, e01535.

13  G. C.-T. Wei, *J. Am. Ceram. Soc.*, 1983, **66**, C111–C113.

14  SICAT Catalyst, 2022, Official Web Site, accessed 03 May, https://www.sicatcatalyst.com/.

15  H. J. Kitchen, S. R. Vallance, J. L. Kennedy, N. Tapia-Ruiz, L. Carassiti, A. Harrison, A. G. Whittaker, T. D. Drysdale, S. W. Kingman and D. H. Gregory, *Chem. Rev.*, 2014, **114**, 1170–1206.

16  S. L. James, C. J. Adams, C. Bolm, D. Braga, P. Collier, T. Friščić, F. Grepioni, K. D. M. Harris, G. Hyett, W. Jones, A. Krebs, J. Mack, L. Maini, A. G. Orpen, I. P. Parkin, W. C. Shearouse, J. W. Steed and D. C. Waddell, *Chem. Soc. Rev.*, 2012, **41**, 413–447.

17  L. Takacs, *Chem. Soc. Rev.*, 2013, **42**, 7649–7659.

18  S. Eilbeigi, S. A. Hassanzadeh-Tabrizi and A. Khodaivandi, *Ceram. Int.*, 2018, **44**, 21437–21441.

19  M. Semnan and M. Jalaly, *Mater. Res. Express*, 2016, **3**, 115018.

20  R. Wu, K. Zhou, C. Y. Yue, J. Wei and Y. Pan, *Prog. Mater. Sci.*, 2015, **72**, 1–60.

21  P. Nguyen and C. Pham, *Appl. Catal., A*, 2011, **391**, 443–454.

22  D. L. Nguyen, P. Leroi, M. J. Ledoux and C. Pham-Huu, *Catal. Today*, 2009, **141**, 393–396.

23  J. M. García-Vargas, J. L. Valverde, J. Díez, F. Dorado and P. Sánchez, *Int. J. Hydrog. Energy*, 2015, **40**, 8677–8687.

24  Z. Wei, M. Endo, K. Wang, E. Charbit, A. Markowska-Szczupak, B. Ohtani and E. Kowalska, *Chem. Eng. J.*, 2017, **318**, 121–134.

25  H. Li, Y. Qiu, C. Wang, X. Huang, T. Xiao and Y. Zhao, *Catal. Today*, 2018, **317**, 76–85.

26  Y. Song, E. Ozdemir, S. Ramesh, A. Adishev, S. Subramanian, A. Harale, M. Albuali, B. A. Fadhel, A. Jamal, D. Moon, S. H. Choi and C. T. Yavuz, *Science*, 2020, **367**, 777–781.

27  W. J. Jang, J. O. Shim, H. M. Kim, S. Y. Yoo and H. S. Roh, *Catal. Today*, 2019, **324**, 15–26.

28  J.-C. Seo, H. Kim, Y.-L. Lee, S. Nam, H.-S. Roh, K. Lee and S. B. Park, *ACS Sustainable Chem. Eng.*, 2021, **9**, 894–904.

29  S. Sorcar, J. Das, E. P. Komarala, L. Fadeev, B. A. Rosen and M. Gozin, *Mater. Today Chem.*, 2022, **24**, 100765.

30  W. Liu, L. Li, S. Lin, Y. Luo, Z. Bao, Y. Mao, K. Li, D. Wu and H. Peng, *J. Energy Chem.*, 2022, **65**, 34–47.

31  K. Y. Kim, J. H. Lee, H. Lee, W. Y. Noh, E. H. Kim, E. C. Ra, S. K. Kim, K. An and J. S. Lee, *ACS Catal.*, 2021, **11**, 11091–11102.

32  J. Niu, Y. Wang, S. E. Liland, S. K. Regli, J. Yang, K. R. Rout, J. Luo, M. Rønning, J. Ran and D. Chen, *ACS Catal.*, 2021, **11**, 2398–2411.

33  Y. Guo, M. Castiñeira Reis, J. Kootstra and S. R. Harutyunyan, *ACS Catal.*, 2021, **11**, 8476–8483.

34  X. Li, D. Li, H. Tian, L. Zeng, Z. J. Zhao and J. Gong, *Appl. Catal., B*, 2017, **202**, 683–694.

35  Q. Zhang, M. Sun, P. Ning, K. Long, J. Wang, T. Tang, J. Fan, H. Sun, L. Yin and Q. Lin, *Appl. Surf. Sci.*, 2019, **469**, 368–377.

36  K. Bu, J. Deng, X. Zhang, S. Kuboon, T. Yan, H. Li, L. Shi and D. Zhang, *Appl. Catal., B*, 2020, **267**, 118692.

37  L. Xu, F. Wang, M. Chen, X. Fan, H. Yang, D. Nie and L. Qi, *J. CO2 Util.*, 2017, **18**, 1–14.

38  S. Zhang, S. Muratsugu, N. Ishiguro and M. Tada, *ACS Catal.*, 2013, **3**, 1855–1864.

39  Z. Li, Y. Kathiraser and S. Kawi, *ChemCatChem*, 2015, **7**, 160–168.

40  H. Li, Y. Qiu, C. Wang, X. Huang, T. Xiao and Y. Zhao, *Catal. Today*, 2018, **317**, 76–85.

41  P. Leroi, E. Madani, C. Pham-Huu, M. J. Ledoux, S. Savin-Poncet and J. L. Bousquet, *Catal. Today*, 2004, **91–92**, 53–58.

42  M. Lacroix, L. Dreibine, B. de Tymowski, F. Vigneron, D. Edouard, D. Bégin, P. Nguyen, C. Pham, S. Savin-Poncet, F. Luck, M. J. Ledoux and C. Pham-Huu, *Appl. Catal., A*, 2011, **397**, 62–72.

43  G. Kresse and J. Furthmüller, *Comput. Mater. Sci.*, 1996, **6**, 15–50.

44  J. P. Perdew, K. Burke and M. Ernzerhof, *Phys. Rev. Lett.*, 1996, **77**, 3865–3868.

45  R. Costanza, R. d'Arge, R. de Groot, S. Farber, M. Grasso, B. Hannon, K. Limburg, S. Naeem, R. V. O'Neill, J. Paruelo, R. G. Raskin, P. Sutton and M. van den Belt, *Nature*, 1997, **387**, 253–260.